AFRL-AFOSR-VA-TR-2023-0309

Perylene bisimide-conjugated oligomer dyes

Ziolo, Ronald
CIQA
BLVD ENRIQUE REYNA HERMOSILLO NO.140
SALTILLO, , 25252
MX

03/17/2023
Final Technical Report

Air Force Research Laboratory
Air Force Office of Scientific Research
Arlington, Virginia 22203
Air Force Materiel Command

REPORT DOCUMENTATION PAGE

PLEASE DO NOT RETURN YOUR FORM TO THE ABOVE ORGANIZATION.

1. REPORT DATE	2. REPORT TYPE	3. DATES COVERED	
20230317	Final	START DATE 20210715	END DATE 20220714

4. TITLE AND SUBTITLE
Perylene bisimide-conjugated oligomer dyes

5a. CONTRACT NUMBER	5b. GRANT NUMBER	5c. PROGRAM ELEMENT NUMBER
	FA9550-20-1-0094	
5d. PROJECT NUMBER	**5e. TASK NUMBER**	**5f. WORK UNIT NUMBER**

6. AUTHOR(S)
Ronald Ziolo

7. PERFORMING ORGANIZATION NAME(S) AND ADDRESS(ES)
CIQA
BLVD ENRIQUE REYNA HERMOSILLO NO.140
SALTILLO 25252
MX

8. PERFORMING ORGANIZATION REPORT NUMBER

9. SPONSORING/MONITORING AGENCY NAME(S) AND ADDRESS(ES)	10. SPONSOR/MONITOR'S ACRONYM(S)	11. SPONSOR/MONITOR'S REPORT NUMBER(S)
Air Force Office of Scientific Research 875 N. Randolph St. Room 3112 Arlington, VA 22203	AFRL/AFOSR IOS	AFRL-AFOSR-VA-TR-2023-0309

12. DISTRIBUTION/AVAILABILITY STATEMENT
A Distribution Unlimited: PB Public Release

13. SUPPLEMENTARY NOTES

14. ABSTRACT
The syntheses of three new series of nonlinear optical hyperconjugated macromolecular systems consisting of 4,4-difluoro-4-bora-3a,4a-diaza-s-indacene (BODIPY) dyes functionalized with diverse aryls of thiophenes, carbazoles and perylene bisimides that yield conjugated oligomers with electron attractor character and tunable emission properties was accomplished. The three series of oligomers were synthetized by the step-by-step approach. On basis of the preliminary survey of the photophysical properties and simulated frontier
molecular orbitals here presented, these conjugated molecular-based functional organic dyes offer a vast chemical space to be explored to tune the optoelectronic properties. From the so synthetized materials, the perylene bisimide derivatives exhibit the most appealing
optoelectronic properties towards the proposed application:
1) good solubility in many organic solvents,
2) strong absorptions in the red region,
3) broad fluorescence covering from 500 to 800 nm,
3) push-pull character,
and 4) low lying excited triplet state (as calculated at TD-DFT level), which opens the possibility to have triplet-triplet energy transfer by using AFRL photon donor materials in supramolecular assemblies by physical mixing. A deep photophysical investigation, in particular in the ultrafast domain, is required to establish the most adequate photon donor and nonlinear application.

15. SUBJECT TERMS

16. SECURITY CLASSIFICATION OF:			17. LIMITATION OF ABSTRACT	18. NUMBER OF PAGES
a. REPORT	b. ABSTRACT	c. THIS PAGE		
U	U	U	SAR	24

19a. NAME OF RESPONSIBLE PERSON	19b. PHONE NUMBER *(Include area code)*
STACY MANNI	0000 0000

Standard Form 298 (Rev.5/2020)
Prescribed by ANSI Std. Z39.18

Final Report

Air Force Office of Scientific Research (AFOSR)

Project FA9550-20-1-0094

October 12, 2022

Perylene Bisimide-Conjugated Oligomer Dyes as Versatile Supramolecular Architectures For Functional Optoelectronic Devices

Eduardo Arias (coPI), Ivana Moggio (coPI), Ronald F. Ziolo (coPI/PD)

eduardo.arias@ciqa.edu.mx, ivana.moggio@ciqa.edu.mx

rziolo@cs.com

Centro de Investigación en Química Aplicada (CIQA)

Blvd. Enrique Reyna, No. 140, 25294,

Saltillo, Coahuila, México

Summary of Accomplishments

The syntheses of three new series of nonlinear optical hyperconjugated macromolecular systems consisting of 4,4-difluoro-4-bora-3a,4a-diaza-s-indacene (BODIPY) dyes functionalized with diverse aryls of thiophenes, carbazoles and perylene bisimides that yield conjugated oligomers with electron attractor character and tunable emission properties was accomplished. The three series of oligomers were synthetized by the step-by-step approach. On basis of the preliminary survey of the photophysical properties and simulated frontier molecular orbitals here presented, these conjugated molecular-based functional organic dyes offer a vast chemical space to be explored to tune the optoelectronic properties. From the so synthetized materials, the perylene bisimide derivatives exhibit the most appealing optoelectronic properties towards the proposed application: 1) good solubility in many organic solvents, 2) strong absorptions in the red region, 3) broad fluorescence covering from 500 to 800 nm, 3) push-pull character, and 4) low lying excited triplet state (as calculated at TD-DFT level), which opens the possibility to have triplet-triplet energy transfer by using AFRL photon donor materials in supramolecular assemblies by physical mixing. A deep photophysical investigation, in particular in the ultrafast domain, is required to establish the most adequate photon donor and nonlinear application.

Motivation and Impact

Conjugated molecular-based functional nanomaterials such as organic dyes are particularly important since, in comparison to crystalline solids, they offer a vast chemical space to be explored. Moreover, nonlinear absorption (NLA) represents a specific technical application where this aspect has proven essential and enabling. Several strategies have emerged to tune the photo-physical properties of such molecules and improve their NLA behavior including varying the conjugation length, changing the character of the conjugated bridge, increasing the planarity of the chromophore, increasing the length of the π-conjugated system, dendrimer and glass encapsulation, and/or incorporating different metals.

In this project, we proposed basic science which may support several applications having Air Force relevance. There is a requirement for materials for laser protection that respond in the near infrared and beyond and have excited state lifetimes up to seconds. As such, donor-acceptor materials, including donor materials from AFRL and acceptors from CIQA, are candidate materials for this application. Some of the AFRL materials have been shown to efficiently produce triplet excitons upon illumination with platinum(II)-containing phenyleneethynylene oligomers. Illumination of these materials in the presence of acceptors which have long excited state lifetimes may produce stable spins which can be manipulated for spintronics applications. In the proposal, we visualized, that the project also has potential relevance in the field of quantum communication by preparing emitters which potentially produce entangled photons. To this end, in this project, we proposed the syntheses of a series of 4,4-difluoro-4-bora-3a,4a-diaza-s-indacene (BODIPY, see following structure) dyes functionalized with diverse aryls such as thiophenes, perylene bisimides and/or lanthanide complexes in order to obtain conjugated oligomers with electron attractor character but also with possible excited state lifetimes up to nanoseconds.

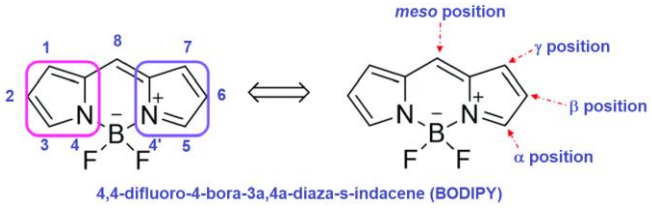

Three series of oligomers were synthetized by the step-by-step approach.

Changes / Delays

Mexican government mandated lab closures due to Covid pandemic limited CIQA laboratory time on the project to about one year. AFRL in the U.S. was unable to collaborate and follow through with expected materials delivery, testing and further characterizations. Quarantine, limitations and communications at AFOSR/SOARD interfered with CIQA extension request.

1) Synthesis of BODIPY- thiophenes

The first series is mainly composed of BODIPY as core and functionalized with thiophenes in *meso*- and in 2,6 positions by single or triple bonds, Chart 1.

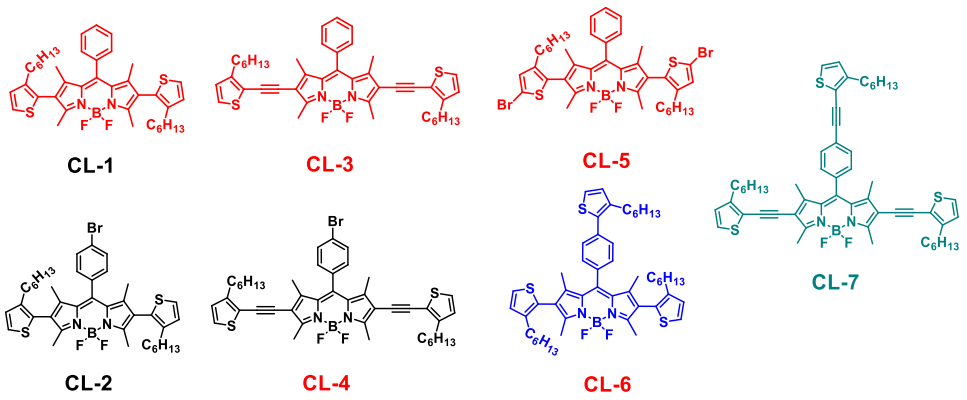

Chart 1. BODIPY as core and functionalized with thiophene in diverse positions.

The strategy consisted in synthesizing a series of functional BODIPY monomers and then to achieve a palladium cross-coupling reaction with thiophenes by the Sonogashira or Suzuki reaction conditions to obtain the conjugated oligomers. Scheme 1 depicts the pathway used to obtain the required monomers.

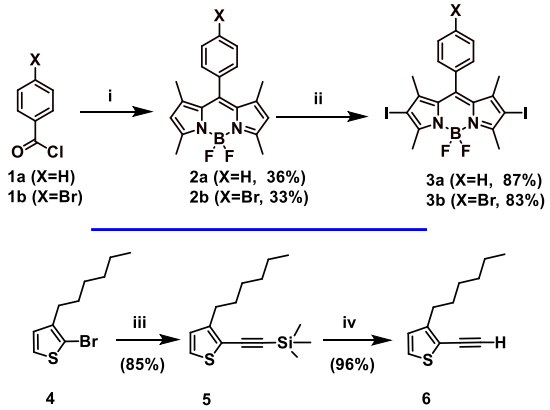

Scheme 1. Reaction conditions: i) 2,4-dimethylpyrrole, CH_2Cl_2, r.t., 16 h, Et_3N, $BF_3{\cdot}Et_2O$, 2h; ii) NIS, CH_2Cl_2, r.t., 30 min; iii) TMSA, $Pd(PPh_3)_2Cl_2$ (5% mol), CuI (1.5% mol), Et_3N ,80°C, 16 h; iv) TBAF (1 M in THF), THF, H_2O, SiO_2,15 min.

The step for obtaining BODIPY monomers with a phenyl (**3a**) or *p*-bromophenyl (**3b**) substituent at the *meso* position is as follows: benzoyl chloride **1a** (or 4-bromo benzoyl chloride **1b**) was condensed with 2-4 dimethylpyrrole at room temperature overnight, followed by a boron complexation with $BF_3{\cdot}Et_2O$ and triethylamine as a base to obtain **2a** and **2b**, respectively. **2a** and **2b** were selectively iodinated with N-iodosuccinimide (NIS) in position 2 and 6 affording **3a** and **3b** in yields around 85 %. Conversely, the commercially available 2-bromo-3-hexylthiophene

4 was subjected to a Sonogashira cross coupling reaction with trimethylsilylacetylene (TMSA) to obtain (3-hexylthiophen-2-yl) trimethylsilylethynylene **5,** which later underwent desilylation with tetrabutylamonium fluoride (TBAF) to obtain the desired (3-hexylthiophen-2-yl) ethynylene **6**. The oligomers were designed to assess the influence of a bromide group and ethynyl bridges on the photophysical properties of BODIPY-thiophene oligomers. The inclusion of a bromide group enhances the intersystem crossing which may influence the triplet state population. Another design strategy used is the extension of the conjugation with ethynyl bridges which should promote a more delocalization of π electrons through the molecule. The synthetic pathway used for obtaining thiophene-BODIPY-thiophene oligomers is depicted in Scheme 2. **Error! Reference source not found.**The oligomers **CL-1** and **CL-4** resulted from a Suzuki-Miyaura cross-coupling reaction of monomer **3a** or **3b** (1 eq.) with 3-hexylthiophene-2-boronic acid pinacol ester (2.2 eq.). In the case of **CL-4** Suzuki-Miyaura reaction, stoichiometry along with high reactivity of iodide groups promoted coupling predominantly at 2 and 6 positions in the BODIPY moiety with moderate yield ca. 55%. **3a** (**3b**) substituted with one thiophene was also formed but in very low yield <4%, which could be isolated by preparative GPC (Biorads, Bio-Beds SX1, toluene). No traces of tri-substituted thiophenes in **3a** or **3b**, with the structure of **CL-6,** was isolated or recovered during the purification. Actually, bromine in *meso*-phenyl is only very moderately reactive to Pd cross coupling reactions. The BODIPY-thiophene oligomer **CL-3** connected through ethynylene bridges was obtained via Sonogashira cross coupling reaction of **3a** (1eq.) with **6** (2 eq.). In the case of **CL-5**, the Sonogashira reaction was carried out by the Godt's procedure [1] where the iodine group reacts preferentially with acetylenes at 0°C, while bromine requires heating. **CL-6** was obtained by reacting **3b** (1 eq.) with 3-hexylthiophene-2-boronic acid pinacol ester (4 eq.), while for **CL-7** formation, **3b** (1eq.) was reacted with **6** (4 eq.), but as was previously mentioned, bromine in *meso*-phenyl is very moderately reactive and excess of reactants are necessary to completely obtain the respective oligomers.

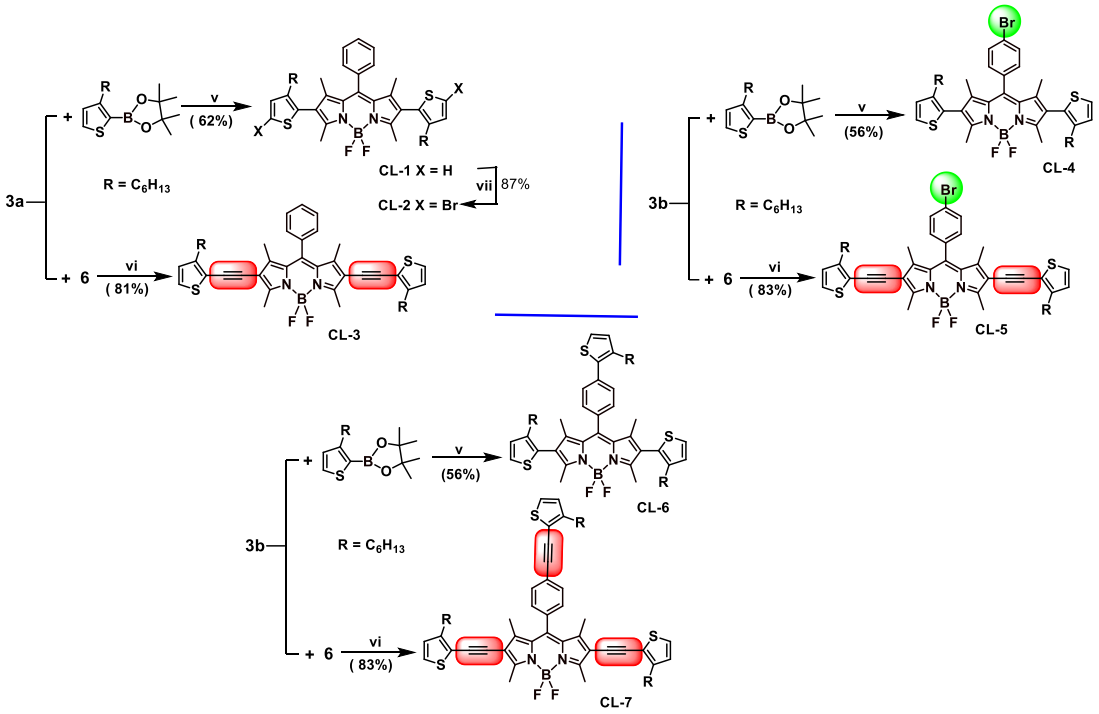

Scheme 2. Reaction conditions. v) 3-hexylthiophene-2-boronic acid pinacol ester, $Pd(PPh_3)_2Cl_2$ (5% mol), THF, Na_2CO_3 aq (0.78M), 70°C, 16 h; vi) 6, $Pd(PPh_3)_2Cl_2$ (5% mol), CuI (1.5% mol), THF, Et_3N ,70°C (0° to rt for 8b), 16 h.

Previous to the photophysical, electrochemical and theoretical calculus performed in this project, we realized that BODIPY monomers behaved as rotors, because the ^{1}H and ^{13}C NMR spectra showed displacement of certain aromatic signals as a function of the temperature and concentration. Therefore, it was necessary to determine such behavior because as a measure that the molecular structure got larger in the oligomers, the NMR characterization were more difficult to be interpreted. The results of our study is presented in the Appendix, in an independent two-column format for sake of condensation. It is worth to mention that the photophysical characterization of this BODIPY- thiophenes series is currently being carried out.

2) Synthesis of BODIPYS-Carbazoles

The second series is composed of BODIPY as core and functionalized with carbazoles in *meso*- and or 2,6 positions by single bonds, Chart 2.

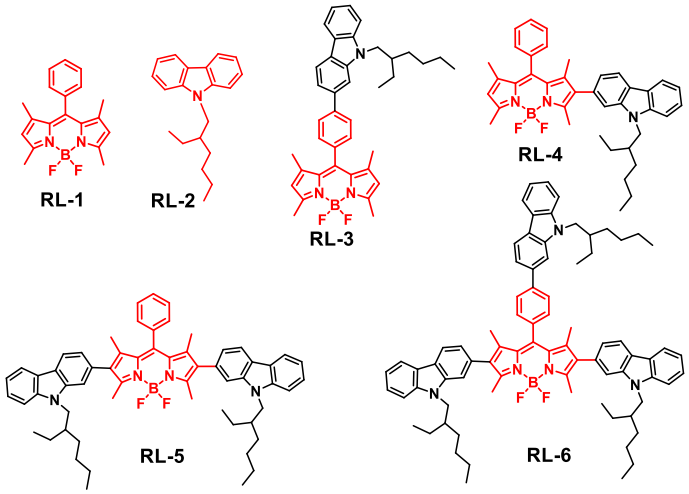

Chart 2. BODIPYs as core and functionalized with carbazole in diverse positions.

The strategy consisted in synthesizing a series of functional monomers, and then to achieve palladium cross-coupling reaction with 9-ethylhexyl-9h-carbazole-3-boronic acid pinacol ester by the Suzuki reaction conditions, to form the conjugated oligomers. Scheme 3 depicts the pathway used to obtain the required monomers.

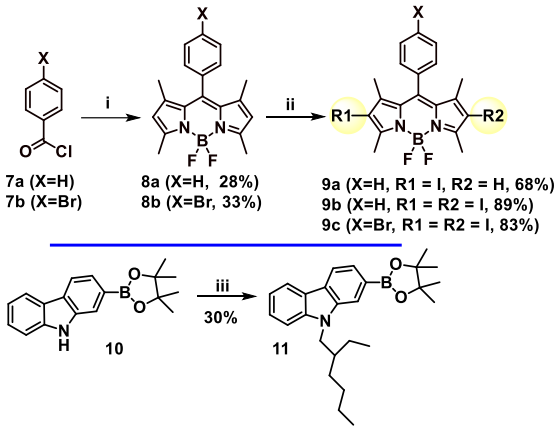

Scheme 3. Reaction conditions: i) 2,4-dimethylpyrrole, CH_2Cl_2, r.t., 16 h, Et_3N, $BF_3{\cdot}Et_2O$, 2h; ii) NIS, CH_2Cl_2, r.t., 30 min; iii) Cs_2Co_3, 2-ethylhexyl bromide, 60 °C, 48 h.

The involved steps for obtaining BODIPY monomers with a phenyl (**9a**) or *p*-bromophenyl (**9b**) substituent at the *meso* position are as follows: benzoyl chloride **7a** (or 4-bromo benzoyl chloride **7b**) was condensed with 2-4 dimethylpyrrole at room temperature overnight, followed by a boron complexation with $BF_3{\cdot}Et_2O$ and triethylamine as a base to obtain **8a** and **8b**, respectively. **8a** and **8b** were selectively mono- or di-iodinated with *N*-iodosuccinimide (NIS) in position 2 or 2,6 by controlling the number of NIS equivalents affording **9a** and **9b** in yields around 80 %. Conversely, the commercially available 9H-carbazole-3-boronic acid pinacol ester **10** underwent

a Williamson alkylation with 2-hethylhexyl bromide and Cs_2Co_3 as base to obtain the desired 9-ethylhexyl-9h-carbazole-3-boronic acid pinacol ester **11** in yields around 30%.

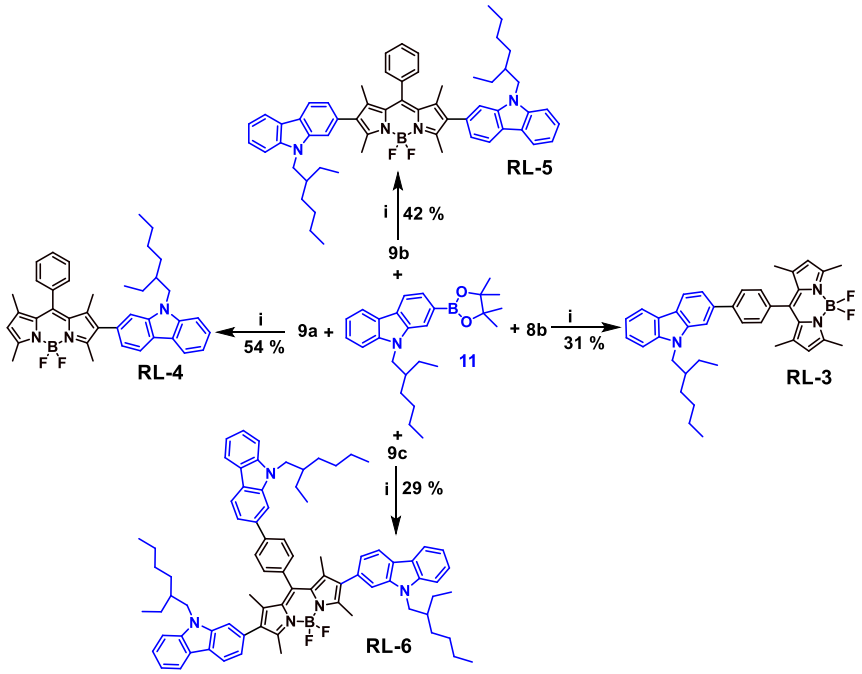

Scheme 4. Reaction conditions: i) $Pd(PPh_3)_2Cl_2$ (5% mol), THF, Na_2CO_3 aq (0.78M), 70°C, 16 h;

The synthetic pathway used for obtain BODIPY-carbazole oligomers is depicted in Scheme 4. The synthesis is based on the Suzuki reaction, from which the 9-ethylhexyl-9h-carbazole-3-boronic acid pinacol ester **11** is cross-coupled with the respective halide-BODIPY **8b-9c**, for instance with **9b** and the 2,6-disubstituted carbazole **RL-5** is formed and so successively with the rest of the structures. We note that, when the reaction involves the cross-coupling of *meso p*-phenyl-BODIPYS **8b,9c** with **11**, yields were always low because of the low reactivity of the Br in this phenyl, likely affected by the inductive effect of the BODIPY. All of the oligomers were subjected to a metal decomplexation with EDTA and then passed through a GPC gravimetric column (Biorads, Bio-Beds SX1, toluene).

2.1 Photophysical properties.

Table 1 presents the photophysical properties of the BODIPY-carbazole macromolecules in chloroform, while Figures 1a and 1b show the corresponding absorption/ fluorescence spectra. The BODIPY **8a** and the carbazol **RL-2** were also analyzed as reference compounds. In general all of the compounds present a main peak, attributed to the S_0-S_1 electronic transition at around 500-540 nm with high extinction coefficient ε (~10^4 $M^{-1}cm^{-1}$) similar to the BODIPY precursor **8a** and in agreement with the literature.[2] The redshift of this peak from 502 nm in the BODIPY reference compound to 517 nm for **RL-4** and to ~540 nm for **RL-5** and **RL-6** reveals that the carbazole substituted in the pyrrol positions of the BODIPy is electronically interacting, i.e. the

conjugation extends in the whole structure; as a consequence, the optical band gap E_g slightly decreases from 2.4 eV to 2.1 eV. On the contrary, when substituted in the *meso*-phenyl, no significant changes in the peak position are found as the meso-phenyl induces the orthogonality of the two chromophores, i.e., the carbazole in the *meso* position relative to the BODIPY (**RL-3** comparative to **8a**) or relative to the BODIPY that has the two carbazoles in the pyrrol (**RL-6** comparative to **RL-5**). As a consequence, there is negligible electronic interactions between the carbazole and the BODIPy at the ground state; similar results were found in literature.[3] Other peaks can be detected in the UV region that can be ascribed to carbazole electronic transitions as in the corresponding reference. The half-height bandwidth HHBW of the main absorption maxima increases correspondingly to the conjugation extension being just 20 nm for **RL-3** where the BODIPY unit is the only absorbing chromophore (as in the model compound), to 28 nm for **RL-4** where the conjugation is extended to one carbazole in pyrrol position and to ~50 nm for **RL-5** and **RL-6** where the BODIPy has two carbazoles in both pyrrols. This trend can be explained on the basis of the larger number of rotamers that can derive from the free rotations around the single bonds of the BODIPY core. The same trend is observed in the fluorescence maxima where the meso-subtitution does not shift the position, while the pyrrol substitution gives a bathochromic effect passing, for instance, from 514 nm for the model compound and **RL-3** to 569 nm for **RL-4** that has only one carbazole at the 2 position and to 592 nm and 597nm for **RL-5** and **RL-6**, which have 2 carbazoles, in the 2,6 positions.

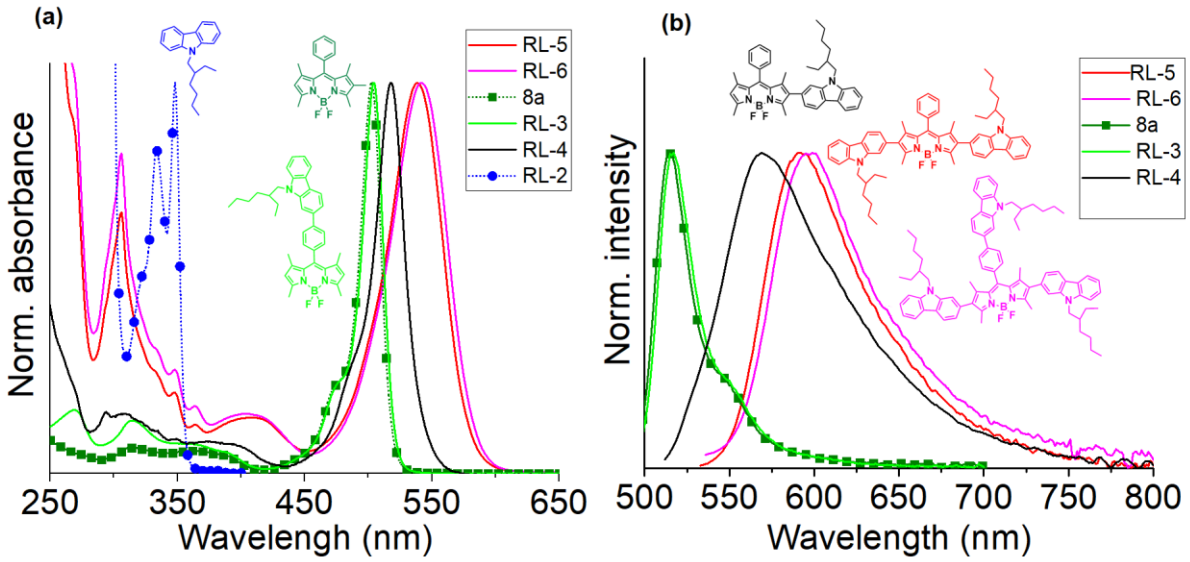

Figure 1. (a) Normalized UV-Vis absorption spectra (10^{-5}-10^{-6} M^{-1}) in chloroform and (b) normalized fluorescence spectra in chloroform of the compounds depicted in Chart 2.

In general, the trend observed in the absorption properties is retained in the fluorescence spectra, Figure 1b: i) the meso-substituted BODIPy **RL-3** presents a sharp (HHBW=25 nm) and structured emission with features that are mirror-like to the S_0-S_1 excitation, and maximum at

516 nm, typical of BODIPys and similar to the reference compound **8a**. Consistently, the Stokes' shift values ($\Delta\nu$~460 nm), in the range of molecules that do not suffer changes in the geometry upon excitation, are very similar as well as are the fluorescence quantum yield ϕ, lifetimes values τ and radiative k_{rad} and non-radiative k_{nr} constants. For the BODIPys bearing the carbazoles in the pyrrol positions, the emission peak turns broader and unresolved and the maximum shifts to the red, with an increasing displacement along with the carbazoles number functionalized in the pyrrol position of the BODIPy and with the same trend found for the absorption maximum: **RL-4<<RL-5<RL-6.** The Stokes' shift values are also much larger for these three compounds relative to the reference BODIPy and to the *meso* functionalized compound. The $\Delta\nu$ of approx. 1700 cm^{-1} indicates a change of the geometry from aromatic to quinoid from the ground to the excited state. Despite to this difference, we can notice that the fluorescence quantum yield for the two derivatives where the BODIPy core is functionalized at both 2 and 6 positions presents practically the same value of the reference (ϕ~0.6), which suggests that the losses due to internal conversion are not the main responsible for the deviation from the unity for the ϕ value. The derivative with just one carbazole has a bit lower ϕ value and a broader emission band. As the two chromophores are directly bonded, electron transfer from the electron donor carbazole to the electron withdrawing BODIPy could occur, and will be further studied.

Table 1. Photophysical properties in $CHCl_3$ of the BODIPY-carbazole macromolecules studied in this work

Oligomer	λ_{abs} [nm]	ε [10^4 $M^{-1}cm^{-1}$]	$HHMW_{abs}$ [nm]	E_g [eV]	λ_{emis} [nm]	$HHBW_{emis}$ [nm]	$\Delta\nu$ [cm^{-1}]	$E_{1,0}$ [eV]	Φ	τ [ns]*	K_{rad} x10^9 [s^{-1}]*	K_{nr} x10^9 [s^{-1}]
RL-5	538	5.6	51	2.1	592	69	1695	2.20	0.57	4.2	0.14	0.10
RL-6	541	5.8	53	2.1	597	70	1734	2.18	0.65	3.8	0.17	0.09
8a	502	6.5	20	2.4	514	25	465	2.44	0.63	2.9	0.22	0.13
RL-3	504	11.3	20	2.4	516 (8a)	25	461	2.43	0.61	2.5	0.24	0.16
RL-4	517	6.5	28	2.2	569	82	1768	2.32	0.40	3.8	0.10	0.16
RL-2	348	0.5	-	-	n.d.	n.d.	n.d.	n.d.	n.d.	n.d.	n.d.	n.d.

3) Synthesis of BODIPYS-perylene bisimide

The synthetic pathway to obtain *N*-2-(4-ethynyl-2-fluorophenyl)-9-*N'*-(1-hexylheptyl) perylene- 3, 4, 9,10-tetracarboxyl bisimide **5** is depicted in scheme 5 and was adapted and modified from the literature. [4] The perylene bisimide **1** was partially alkyl hydrolyzed under alkaline conditions;

care must be taken with both, the temperature that must not be higher to 155°C and the time of reaction of 30 min. The perylenic monoanydride monoimide **2** was recovered by flash chromatography in 40 % yield. The so-obtained product was then condensed with 4-bromo-2-fluoroaniline, allowing to achieve an asymmetrically-substituted perylenic bisimide with a suitable bromine group, at which was cross-coupled with TMSA under the Sonogashira reaction to obtain the sylilated compound **4**. The later underwent desylilation with TBAF to obtain the desired compound **5**.

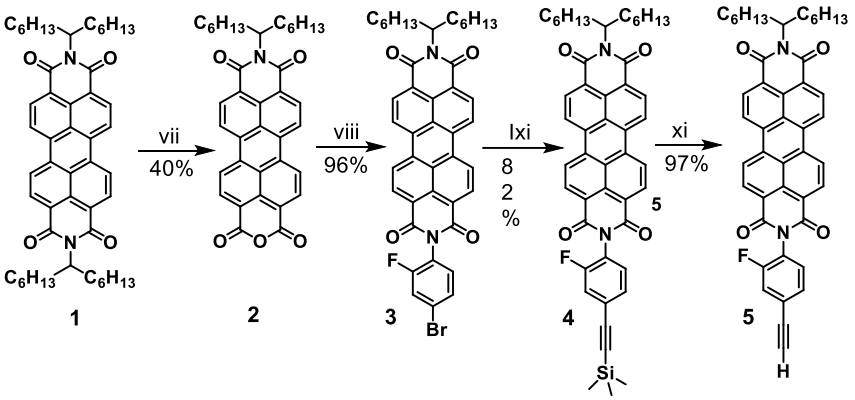

Scheme 5. Reaction conditions: vii) KOH, isopropilic alcohol:water, reflux,then HCl conc., MeOH, 30 min; viii) 4-bromo-2-fluoroaniline, $ZnAc_2$, imidazole, 110° C, 18 h, HCl 2 M, 3 h; ixi) TMSA, $Pd(Ph_3P)_2Cl_2$, CuI, Et_3N, DMF, 80°C, 6h; xi) TBAF (1 M in THF), THF, H_2O, SiO_2, r.t, 15 min.

The thiophene **CL-4** and **CL-2** oligomers previously synthetized in Scheme 2 were used to Sonogashira cross-couple the perylene bisimide **5** dye, Scheme 6. In a first step, **CL-4** was subjected to a cross-coupling Sonogashira reaction with **3** in the *meso*-position affording the dyad **CP-1** in 26 % yields, while the triad **CL-2** was obtained after the cross-coupling reaction of **CL-2** with **5** in 56 % yield.

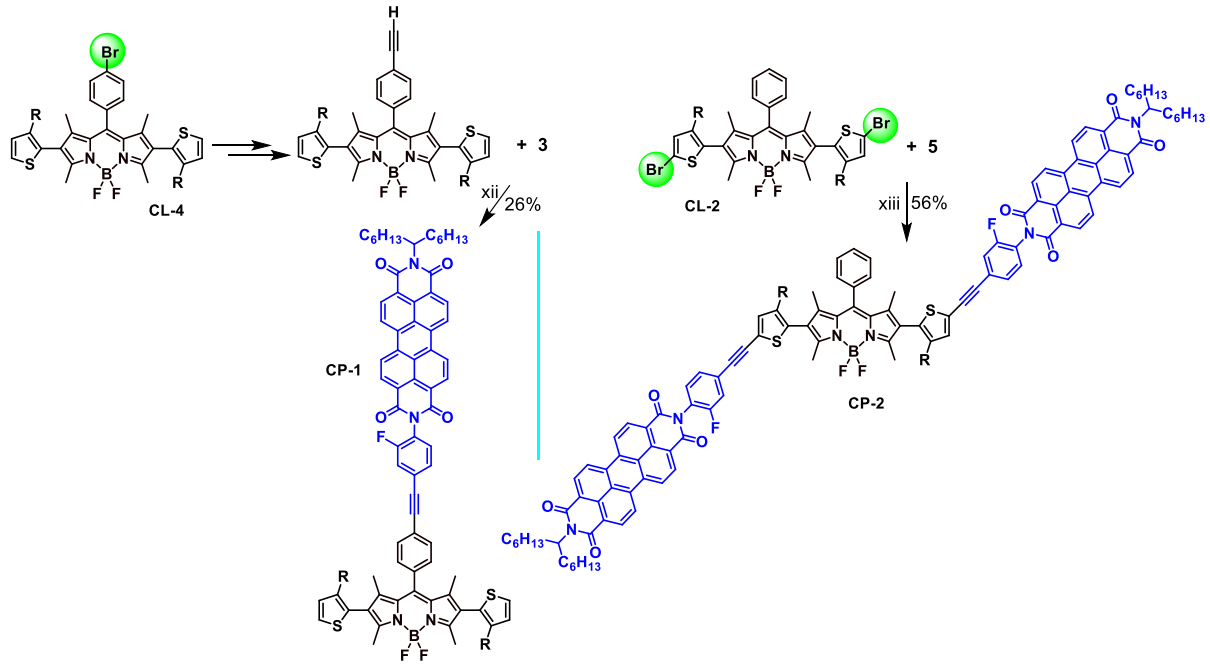

Scheme 6. Reaction conditions: xii) $Pd(PPh_3)_2Cl_2$ (10% mol), CuI (5% mol), DMF, Et_3N, 80 °C, 4 h; xiii) NBS, CH_2Cl_2, r.t.

3.1 Photophysical properties.

The two derivatives **CP-1** and **CP-2** present in the same structure the electron donor *meso*-phenyl BODIPy substituted with thiophene **CL-1** and the electron acceptor perylene bisimide **5** in a dyad and triad structure, respectively. Figure 2 shows their UV-Vis spectra in CH_2Cl_2 together with those of the model compounds: the *meso*-phenyl BODIPY **8a**, **CL-1** and perylene bisimide (**PDI)**.

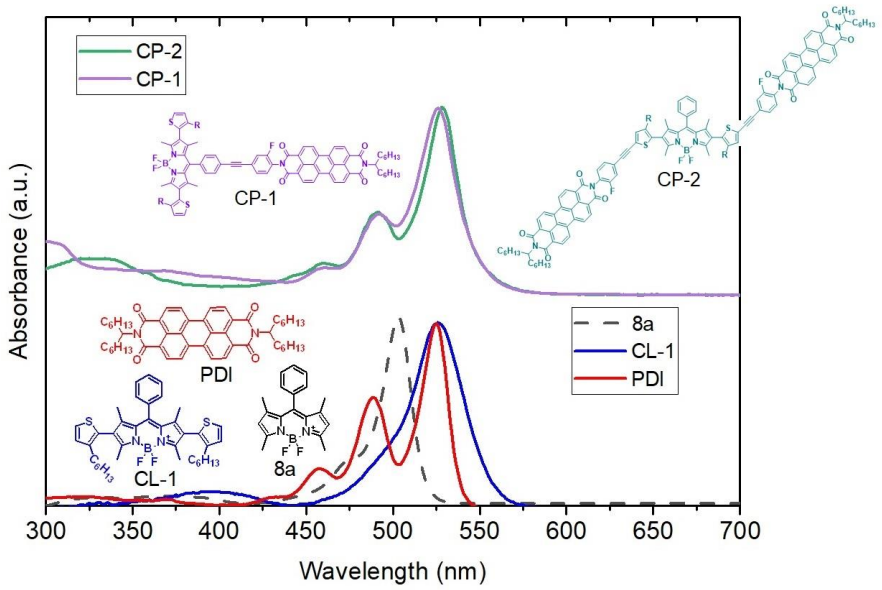

Figure 2. Top potion: UV-Vis spectra of **CP-1**, **CP-2;** bottom portion: the model compounds **8a**, **CL-1** and **1**, in CH_2Cl_2.

The meso phenyl BODIPy **8a** presents a sharp and net peak at 503 nm that can be ascribed to the S_0-S_1 electronic transition, accompanied by its replica at 480 nm, as reported in the literature for BODIPYs. [2] The functionalization in the 2,6 (pyrrol) positions with the thiophene extends the electronic conjugation giving a red shift of the maximum to 523 nm as also observed in similar derivatives.[5] Perylene bisimide also absorbs in this region, with excitonic features being the main S_0-S_1 peak at 526 nm and two replicas at 489 nm and 457 nm. The absorption spectra of the dyad and triad maintain the excitonic features of the precursors where the main absorption is practically at the same wavelength (526 and 528 nm, respectively). Due to the coincidence of the absorption region for the two model compounds, the selective contribution of the two chromophoric units in the overall conjugation, cannot be derived at this level. For a better interpretation of the electronic absorption properties, theoretical simulations have been performed in dichloromethane at def2TZVP/MN15/CPCM level. Figure 3 shows the optimized geometries of the compounds at the ground state and the HOMO, LUMO orbitals. It can be observed that the **CL-1** and perylene bisimide (**PDI)** fragments are orthogonal in **CP-1** and at 45° in **CP-2** because of the phenyleneethynylene spacer and the different BODIPy position in which the **PDI** is functionalized. However, in both cases, the electronic distribution in the HOMO orbital is centered on the **CL-1** fragment, while in the LUMO it is in one of the **PDI** units**,** which suggests that the main absorption presents a charge transfer character in both cases and explains why the maximum has practically the same wavelength.

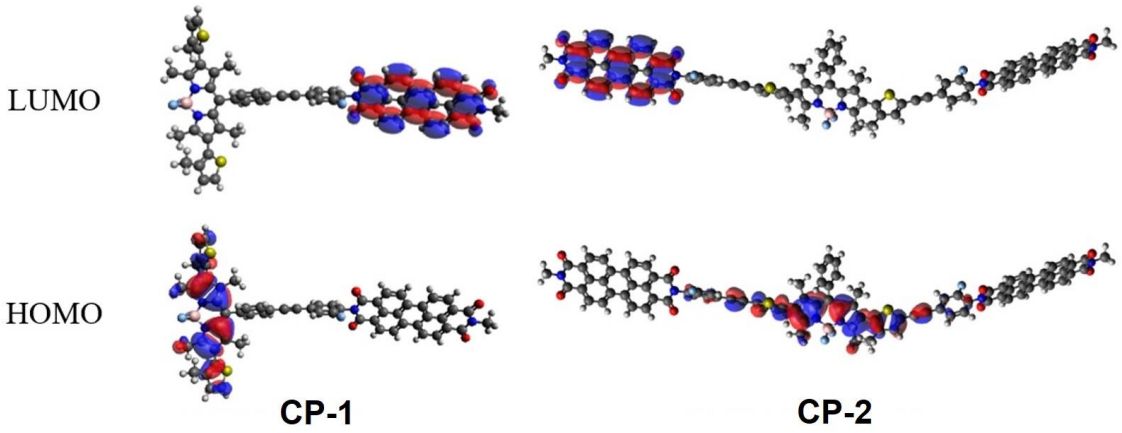

Figure 3. HOMO and LUMO orbitals of **CP-1** (left side) and **CP-2** simulated at def2TZVP/MN15/CPCM level.

Figure 4 presents the fluorescence spectra of the dyad, triad and the corresponding model compounds in CH_2Cl_2.

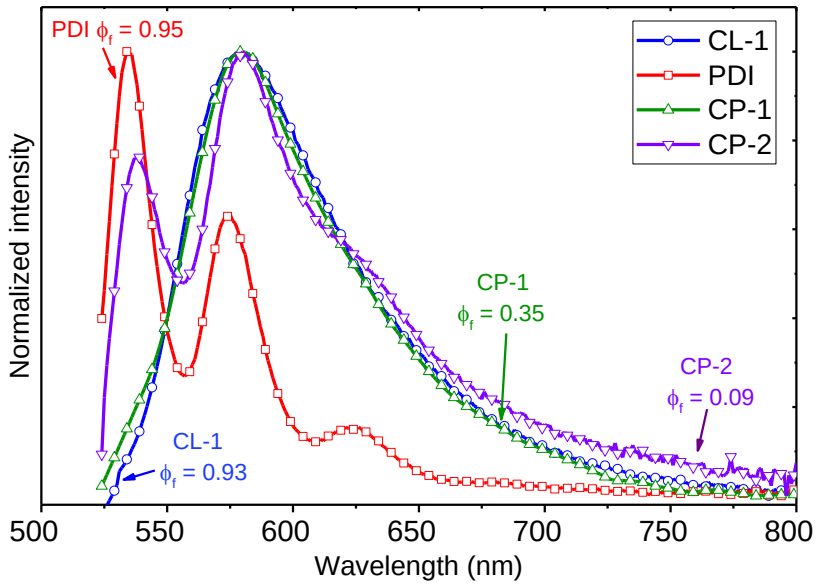

Figure 4. Fluorescence spectra of **CP-1**, **CP-2** and the model compounds **CL-1** and **PDI**, in CH_2Cl_2.

Perylene bisimide **PDI** fluorescence spectrum has excitonic features, mirror-like to the absorption one, with the S_0-S_1 emission at 534 nm, large fluorescence quantum yield (ϕ=0.95) consistent with literature reports. **CL-1** and **CP-1** have practically coincident emission that is broad and not structured with a maximum at 578 nm/580 nm for **CL-1/CP-1** However, the fluorescence quantum yield ϕ is very different from each other, while the model compound has a very high ϕ of 0.93, similar to the mesophenyl BODIPy **8a** (not included), this is strongly quenched in the dyad **CP-1** (ϕ=0.35). Interestingly, **CP-2** has two fluorescence bands; one that

is very sharp and centered at 537 nm, similarly to that of **PDI**, and another one at 580 nm, which is broad and appears similarly to **CL-1**, but the ϕ is almost null (0.09). The fluorescence quenching in the dyad and triad could be due to energy or electron transfer. Energy transfer is a possible de-excitation pathway because of the overlap between absorption of the photon donor segment and emission of the photon acceptor unit as can be observed in Figure 5 taking in account that **CL-1** is the donor and **DPI** is the acceptor, but the extent is estimated to be very low (11%).

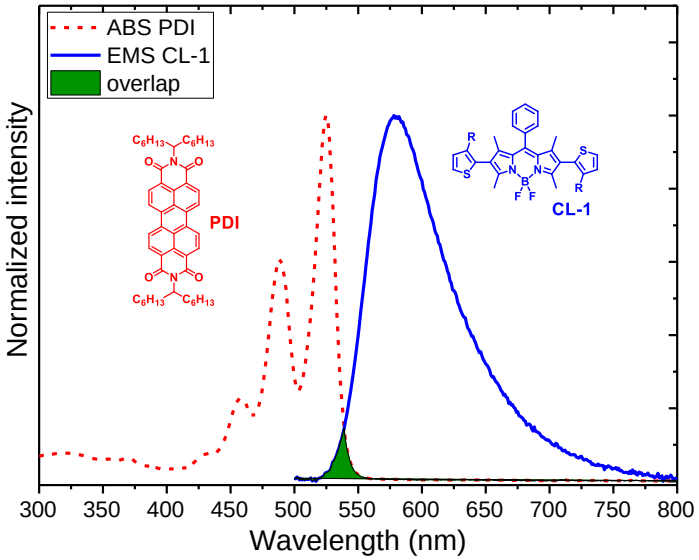

Figure 5. Normalized absorption of the photon acceptor unit (**PDI**) and fluorescence spectrum of the photon donor (**CL-1**) moiety that constitute **CP-1** and **CP-2** in CH_2Cl_2. Spectral overlap is marked in green.

Charge transfer is also possible as a de-excitation process that competes with fluorescence; indeed, the Gibbs free energy in dichloromethane, calculated from the Rehm Weller equation and using the photophysical and electrochemical data, is negative (-0.78 eV for **CP-1** and -0.75 eV for **CP-2)** and the energy for the corresponding charged state is 1.50 and 1.55 eV respectively.

The push pull character of both compounds lowers the energy of the first singlet excited states with respect to the two chromophore units, as observed with the red shift of the absorption peaks. Interestingly, also the energy of the first triplet state is quite low, as estimated by TD-DFT, being 1.29 eV/1.30 eV for **CP-1**/**CP-2,** which matches the requirement as triplet acceptor**.** This could allow further quenching of the fluorescence, through phosphorescence (expected at around 950 nm, not determined) according to the energetic diagram of Figure 6. Excitation on the **PDI** segment can rise to **PDI** fluorescence (observed band at 534 nm) and, through energy transfer, to **CL-1** fluorescence at 580 nm. As the charged state is situated at lower energy compared to both singlet states, the de-excitation crosses this level causing fluorescence quenching, by direct or indirect (after energy transfer) charge transfer. The position of the fist triplet state is below the

charged state, so that this can work as a further photon funnel and finally yields phosphorescence, expected in the NIR region. Further photophysical studies, mainly focused to transient spectroscopy, will be performed at AFRL as originally programmed in the proposal, to corroborate this panorama.

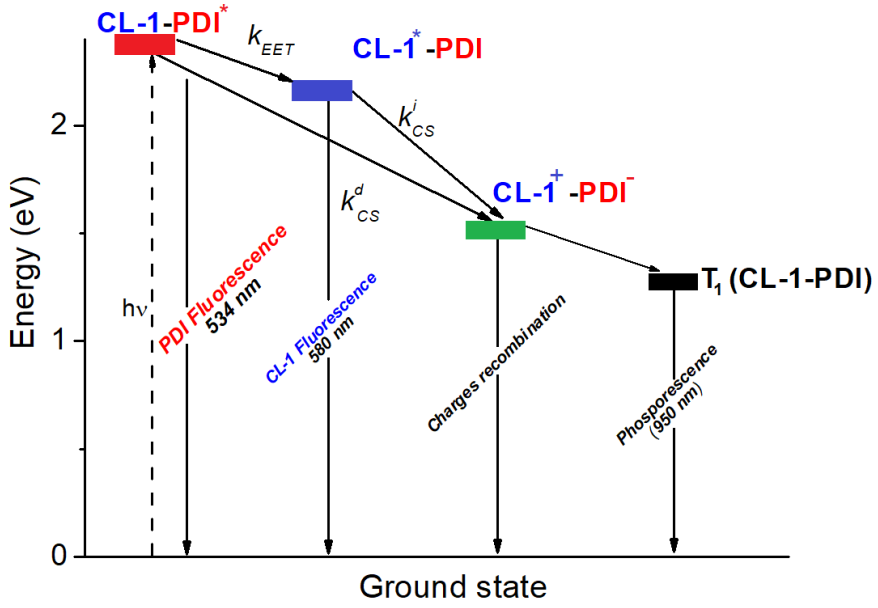

Figure 6. Energy diagram showing proposed photophysical pathways for **CP-2** triad, in CH_2C_{l2}.

Personnel involved in this project other than PIs	**Congress participation:**
Dra. Raquel Ledezma Rodríguez, Technician Dra. Geraldine Rodríguez Riojas, Technician Dr. Gleb Turlakov: Posdoc, 2020-2022 **Thesis** Durán Cázares Jesús Enrique: B.Sc., 2021 Manuel Antonio López Castillo: M.Sc., October 2022 Julio César Valdivia: Ph.D., December 2022 Celín Lozano-Pérez: Ph.D., November 2022	**1)** X-Simposio Nacional de Ingeniería Química y Bioquímica Aplicada, September21 – 23,2022, Matehuala, S.L.P., México. **2)** National Congress of the Polymer Society of México, October 27 to 31, 2022, Monterrey, N.L., México.

Equipment

Independent of the NMR *meso*-BODIPY reorientation study above, ^{1}H (300 MHz) and ^{13}C (75.4 MHz) NMR spectra were obtained at room temperature with a Jeol Eclipse spectrometer using $CDCl_3$ as solvent and taking the remaining non-deuterated chloroform signal as internal reference. MALDI-TOF mass spectra were obtained on a

Bruker Autoflex Speed TOF/TOF operated in reflector mode and using a DCTB matrix in the positive ion mode, sodium trifluoroacetate or NaCl was used as cationized agent. The photophysical properties were analyzed in an acclimatized room (17°C) in spectroscopic dichloromethane. UV-Vis spectra were obtained with a Shimadzu 2401 PC UV/VIS spectrophotometer. The extinction coefficient ε was obtained from the slope of the absorbance vs. molar concentration of at least four solutions. Optical band gap (Eg) was calculated from the intercept with the wavelength axis (in energy values) and the tangent to the normalized absorption spectra at the absorbance of 0.1. The excitation and emission spectra were obtained with a Horiba PTI Quantamaster QM-8450-22-c spectrofluorimeter, equipped with an integrating sphere for the determination of the quantum yield. All the spectra were obtained with background correction and with the same slits and bias between the sample and the solvent. Slits were established in order to keep the uncorrected spectra under the linear range of detection (10^6 counts). The excitation wavelength was 10 nm below the main absorption peaks and the absorbance at that wavelength was adjusted to be lower than 0.1. At least four solutions were analyzed for each complex and the quantum yield was averaged and reported as ϕ in the following. Stokes' shift ($\Delta\nu$) values were calculated from the absorption and fluorescence maximums in wavenumbers (νemis-νabs). Average fluorescence lifetimes τ were obtained by the time correlated single photon counting (TCSPC) technique on a Horiba Jobin Yvon TemPro instrument with a nanoLED laser of a wavelength close to the wavelength used for the emission spectra. Fits were performed on the DAS6 software of the instrument. Radiative (kr) and non-radiative (knr) constants were calculated from the following equations, $kr=\phi/\tau$ and $knr=(1-\phi)/\tau$. A 0.01% suspension of Ludox AS40 (Aldrich) in ultrapure water was used for the prompt signal. Calibration of the equipment was realized with a POPOP [4-bis(4-methyl-5-phenyl-2-oxazolyl)benzene] methanol solution (optical density 0.1 and lifetime of 0.93 ns).[6] The electrochemical properties of all of the compounds were investigated via cyclic voltammetry in a Stand cell from Basi, coupled to an ACM Gill AC potentiostat/galvanostat. The system consisted of a conventional three-electrode cell: glassy carbon as a working electrode (polished with alumina and diamond powder after each run), Pt wire as the counter electrode, Ag/AgCl as reference electrode (viability of -35 $\pm$ 20 mV against the Calomel electrode). Voltammetry measurements were performed at room temperature in dry CH_2Cl_2 containing Bu_4NPF_6 (0.1M) as the supporting electrolyte.

Appendix

STUDY OF THE MOLECULAR REORIENTATION DYNAMICS IN *meso*-PHENYL BODIPYs BY NMR SPECTROSCOPY

Abstract

BODIPY-based fluorescent molecular rotors (FMR) can be used as temperature or viscosity sensors given that the intramolecular rotation can tailor the emission intensity or fluorescence lifetime. Besides fluorescence anisotropy, the molecular reorientation can be assessed by NMR longitudinal relaxation time (T_1). This work focuses on the study by NMR of the molecular reorientation of *meso*-phenyl BODIPY with free and restricted motion. Specifically, ^{1}H T_1 and ^{13}C T_1 were determined by temperature variation from 300 K to 240 K and rotational correlation time (τ_c) along with rotational reorientation activation energy (E_a), which were estimated by the Bloembergen-Purcell-Pound (BPP) theory. In addition, the theoretical chemical shifts were calculated by GIAO-DFT with high correlation (R^2 ~ 0.99 ^{1}H and R^2 ~ 0.97 ^{13}C). The values of ^{1}H T_1 and ^{13}C T_1 diminish with the temperature reduction without reaching a minimum and ^{1}H T_1 values range from 1 to 10 s, while ^{13}C T_1 are from 0.5 to 2 s. BODIPYs show a main rotation axis across the *meso*-phenyl moiety and an anisotropic motion is observed in molecules with free rotation *meso*-phenyl groups. The derived parameters from BPP theory confirmed the high mobility of free rotation *meso*-phenyl groups. These results show the high correlation between structure and molecular reorientation dynamics measured by T_1 NMR

Introduction

BODIPY is a fluorophore with large absorption coefficients in the UV and near infrared region, high fluorescence quantum yield and short fluorescent lifetime, parameters that can be modulated along with functionalization in several positions. [2] These features in BODIPY show potential as molecular fluorescent rotors (FMRs).[7] FMRs have been developed as viscosity and/or temperature sensors given that the intramolecular rotation can tailor the emission intensity or lifetime.[8] Most literature assesses the molecular reorientation in FMRs only by fluorescence anisotropy but NMR spectroscopy can also be used to further study this phenomenon. NMR spectroscopy is a powerful tool to determine the longitudinal relaxation time (T_1), which can be affected by several factors such as electronic effects, molecular mobility and intermolecular interactions.[9,10,11,12] T_1 measurements can show molecular reorientation, segmental and local interactions. Some reported T_1 values in *meso*-substituted BODIPYs with CF_3-terminated alkyl chains are between 2-5 s.[13] However, there are few works that compared the molecular reorientation of *meso*-substituted BODIPY analogues. Therefore, this work studies the molecular reorientation dynamics of

three *meso*-substituted BODIPYs, , by $^{1}HT_1$ and $^{13}CT_1$ and derived parameters from the Bloembergen-Purcell-Pound (BPP) theory.

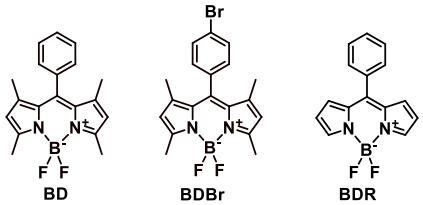

Figure. 1. *Meso*-phenyl BODIPYs studied in this work

Experimental

All chemicals and reagents, from Sigma-Aldrich, were used as received without further purification. The reagents used to synthesize BD, BDBr and BDR (), according to literature procedures, were, benzoyl chloride and 2,4 dimethylpyrrole; 4-bromo benzoyl chloride and 2,4, dimethylpyrrole, benzoyl chloride

and pyrrole. In brief, the reagents were dissolved in fleshly distilled dichloromethane and stirred for 18 h at room temperature. Then triethylamine and $BF_3 \cdot Et_2O$ were added to the flask placed in an ice-water bath and stirred for 2 h. The solution was washed with distilled water and brine and the organic layer was concentrated at low pressure. Column chromatography on silica gel (eluent: 1:1 dichloromethane: n-hexane) provided the product as a red solid.

Chemical shift (δ) assignments of ^1H and ^{13}C experimental spectra were corroborated by computational chemistry with the Gauge-Including Atomic Orbital (GIAO) method. All DFT calculations were performed in ORCA Version 5.0.3.[14] All of the molecular geometries were optimized at def2-SVP/MN15 DFT level and the effects of chloroform were included by the conductor-like polarizable continuum model (CPCM). Shielding constants (σ) were calculated using pcSseg-2 basis set, a triple zeta basis set design for σ calculations, and PBE0 functional. Theoretical displacement δ values were predicted by a linear scaling factor that correlates experimental δ with estimated σ by GIAO-DFT. The coefficient of determination (R^2) was used to assess the theoretical δ.

All NMR experiments were acquired in an AVANCE III HD 400 spectrometer (with a 5 mm multinuclear BBI-decoupling probe with Z grad) with resonance frequencies for ^1H and ^{13}C of 400.14 MHz and 100.61 MHz, respectively. Samples were dissolved in 5 mm Young tubes with $CDCl_3$ (~0.04 g/mL) and de-oxygenated by three freeze-pump-thaw cycles. Measurements were performed between 300 K and 240 K with 10 K cooling ramps and thermal equilibrium time of 300 s. At each temperature ramp, ^1H and ^{13}C spectra were acquired along with T_1 relaxation experiments. The variable delay list (VDLIST) was adjusted for each molecule such that the time interval was between 0.1 T_1 to 1.5 T_1. Typically, VDLIST was 0.1-3 s for both $^1HT_1$ and $^{13}CT_1$ given that only protonated carbons are investigated. The $^1HT_1$ experiments with variable temperature were acquired with delay time of 15 s (D1), a 16 K (TD2) x 10 (TD1) matrix of complex points and 2 accumulated transients per experiment increment. In the case of 13CT1, D1 = 6 s, the complex point matrix was 65 K (TD2) x 7 (TD1) with 180 accumulated transients per experiment increment. $^1HT_1$ and $^{13}CT_1$ data were processed by exponential filter with Fourier transform in F2 dimension with LB = 1Hz for ^1H and 3 Hz for ^{13}C. The integrals used for T_1 calculations in the inversion-recuperation method were performed in the T_1 module of the Dynamic Center software from Bruker using manual integration with one time-constant component.

T_1 values can be explained by a combination of relaxation mechanism. Typically, the relaxation mechanisms for nuclear spin systems are dipole-dipole interactions (DD), chemical shift anisotropy interactions (CSA), spin rotation (SR), scalar coupling (SC) and quadrupolar coupling (Q) [4]. In the case of nuclei with spin ½, contributions from SR, SC and Q can be negligible. The DD relaxation mechanism in ^1H depends mainly of inter or intra molecular neighbor protons. In contrast, $^{13}CT_1$ relaxation is caused by intramolecular DD interactions of carbon-proton bonds. The Bloembergen-Purcell-Pound (BPP) theory provides the theoretical basis for describing the temperature dependence of T_1 observed as a function rotational correlation time (τ_c) and Larmor frequencies. Thus, BPP theory describes DD relaxation for ^1H and ^{13}C with the following equations:

$$\frac{1}{T_{1,H}} = A_{0,H}\left(\frac{\tau_c}{1+(\omega_H\tau_c)^2} + \frac{4\tau_c}{1+(2\omega_H\tau_c)^2}\right) \quad (1)$$

$$X = \left(\frac{\tau_c}{1+((\omega_H-\omega_C)\tau_c)^2} + \frac{3\tau_c}{1+(\omega_C\tau_c)^2} + \frac{6\tau_c}{1+((\omega_C+\omega_H)\tau_c)^2}\right) \quad (2)$$

$$\frac{1}{T_{1,C}} = A_{0,C}(X) \quad (3)$$

$$A_{0,H} = \frac{3N}{10}\left(\frac{\mu_0}{4\pi}\right)\gamma_H^4\hbar(r_{H-H}^{-6}) \quad (4)$$

$$A_{0,C} = \frac{N}{10}\left(\frac{\mu_0}{4\pi}\right)\gamma_C^2\gamma_H^2\hbar(r_{C-H}^{-6}) \quad (5)$$

Where A_0 constant is defined by the number of nuclei attached to the observed nuclei, μ_0 is the vacuum permeability, γ_H and γ_C are ^1H and ^{13}C gyromagnetic constants, h is the reduced Planck constant and r correspond to the proton-proton or C-H distance.

The temperature dependence of rotational correlation time (τ_c) is described by an Arrhenius-type equation.

$$\tau_C = \tau_0 exp\left(\frac{E_a}{RT}\right) \quad (6)$$

Where τ_0 is the preexponential factor, R is the ideal gas constant, T is the absolute temperature, Ea is the molecular reorientation activation energy. Typically, T_1 measurements as a function of temperature allow to determine a minimum which can be correlated with A_0 given that this parameter is temperature independent. In case that a minimum in the temperature range is not observed, τ_c can be calculated by non-linear least squares.[15]

Results and Discussion

The chemical structures of *meso*-phenyl BODIPYs were confirmed by ^{1}H and ^{13}C NMR. The chemical shift (δ) assignment was corroborated by GIAO-DFT where R^2 ~ 0.99 for ^{1}H and ~0.98 for ^{13}C. ^{1}H NMR spectra of BD, BDBr and BDR in *Figure. 2* show similar peaks and intensities for BD and BDBr. For BD and BDBr, methyl protons H10 and H11 are at δ ~ 1.4 ppm and δ ~ 2.6 ppm, while methine protons H2 are at δ ~ 6.0 ppm. In the case of BDR, methine protons H1, H2 and H3 are shifted towards low field and located at 7.9, 6.6 and 6.9 ppm, respectively. In the aromatic region, phenyl protons of BD are observed as two little broad signals at 7.3 ppm (H7, 2H) and 7.5 ppm (H8 and H9, 3H); for BDBr phenyl protons are observed as an AA'BB' spin coupling system at 7.2 ppm (H7, d, J = 8.4 Hz, 2H) and 7.7 ppm (H8, d, J = 8.4 Hz, 2H); and a broad signal at 7.6 ppm (H7, H8 and H9, 5H) for BDR.

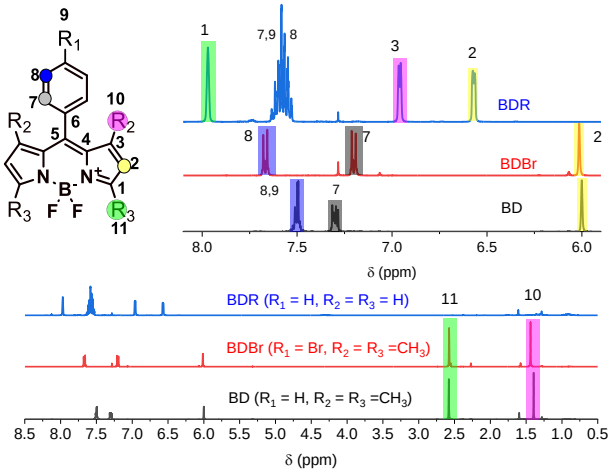

Figure. 2. ^{1}H spectra assignments for meso-phenyl BODIPYs.

The ^{13}C NMR assignment of protonated carbons (C2, C7, C8, C10 and C11) was confirmed by GIAO-DFT as shown in *Figure 3*. The protonated carbons were selected because they have higher intensity than quaternary carbons which is important for ^{13}C T_1 measurements and parameter derivation with BPP theory. C2 methine carbons are observed as single peaks at δ ~ 121 ppm for BD and BDBr, while for BDR C2 it is shifted towards high field (δ ~ 118 ppm). Methyl carbons (C10 and C11) of BD show two signals at δ ~14.3 and 14.6 ppm, while for BDBr only one signal is observed at δ ~14.3 ppm. This behavior is also reproduced by theoretical δ calculations (GIAO-DFT) suggesting that the bromo-phenyl moiety has a deshielding effect over C10. This deshielding effect is also observed for the aromatic carbons C7(δ ~129.8 ppm) and C8 (δ ~132.4 ppm) in BDBr relative to carbons in BD. In BDR, C7, C8 and C9 are observed at δ ~ 130.5, 128.4 and 130.7 ppm, respectively.

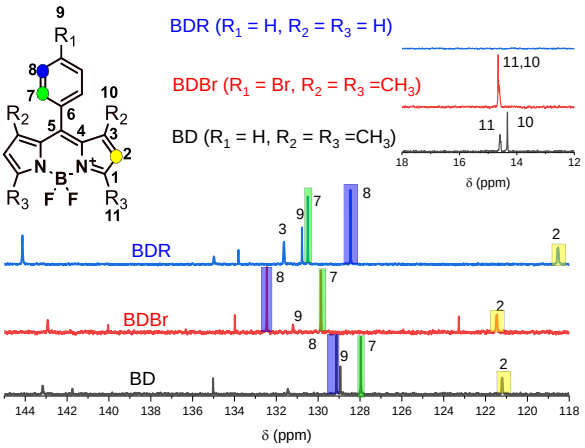

Figure 3. ^{13}C spectra assignments for meso-phenyl BODIPYs.

The $^{1}HT_1$ and $^{13}CT_1$ temperature dependence, Figure. 4, in *meso*-phenyl BODIPY analogues shows that T_1 values diminish with the temperature reduction without reaching a minimum. The absence of a minimum in the range of 300 K to 240 K indicates that the observed nuclei show free rotation along Z axes and the solvent is non-viscous.[16] For example, Figure. 4a shows the temperature dependence of BD from 300 K to 240 K. At 300 K, $^{1}HT_1$ of H11 and H10 in BD is ~ 1.7 s and T_1 values for H7, H8 and H9 are 3.2-4.3 s and for H2 T_1 = 5.3 s. The short $^{1}HT_1$ values in methyl groups are explained by a combination of spin-rotation and dipolar relaxation mechanism where SR is the dominant mechanism [11]. Thus, methyl groups in BD show fast and unrestrained rotational motions with efficient SR relaxation at RT and high temperatures which means shorter T_1 [12]. The long T_1 in H2 is also dominated by a combination of DD and SR mechanism since the closer protons are in the methyl groups and DD relaxation becomes ineffective. It can also be argued that BD tumbles rapidly in solution due to the small molecular weight. Therefore, the dipole-dipole relaxation in H2 is not effective and T_1 becomes longer. In the aromatic region, T_1 of H8 and H9 are shorter than the one in H7 suggesting that H9 is a rotational axis. However, the strong spin-spin coupling (J) in the aromatic region limits further discussion of the molecular motion. Thus, $^{13}CT_1$ measurements were performed

given that the principal relaxation mechanism in carbons with directly attached protons is dipole-dipole.

*Figure. 4*b shows the temperature dependence of $^{13}CT_1$ in BD which shows similar features as $^{1}HT_1$ curves. At 300 K, $^{13}CT_1$ of C10 and C11 is around 1.8 s; for C2, C7, C8 and C9 $^{13}CT_1$ is 1.3, 1.2, 1.3 and 1.1 s, respectively. In this case, the fast and unrestricted motion of methyl groups is represented by long T_1 (1.8 s) given that DD relaxation is less effective, while the phenyl moiety show effective DD relaxation (shorter T_1). $^{13}CT_1$ in C9 is the shortest T_1 compared to C2, C7 and C8. These is because rotation around the axis is fast, and causes inefficient relaxation (long T_1) for the off-axis carbons. With the results from $^{1}HT_1$ and $^{13}CT_1$, we propose that BD behaves as a sphere with an isotropic rotational motion where C9 and B atom are in the rotational axis and C2 is the farthest off-axis carbon, insets in Figure. 4.

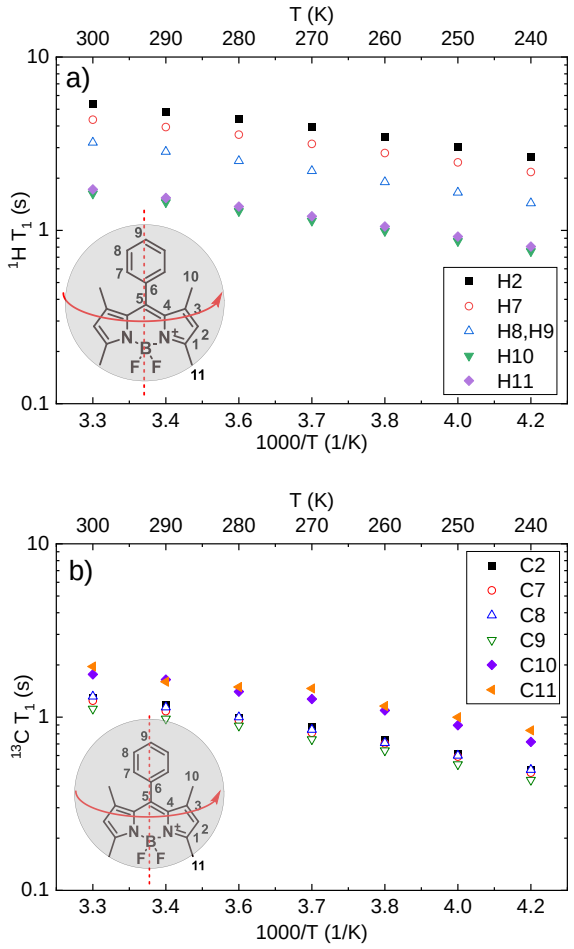

Figure. 4. Temperature dependence of BD. a)$^{1}HT_1$ and b) $^{13}CT_1$. Inset: Proposed rotational motion of BD.

Figure. 5 shows the comparison of $^{1}HT_1$ and $^{13}CT_1$ vs temperature of selected atoms in BD, BDBr and BDR where T_1 values diminish with temperature reduction. This behavior is characteristic of small molecules in non-viscous solvents. Here, the relaxation is less efficient with overall rapid molecular rotation and as temperature diminish the relaxation becomes more effective and T_1 shortens.

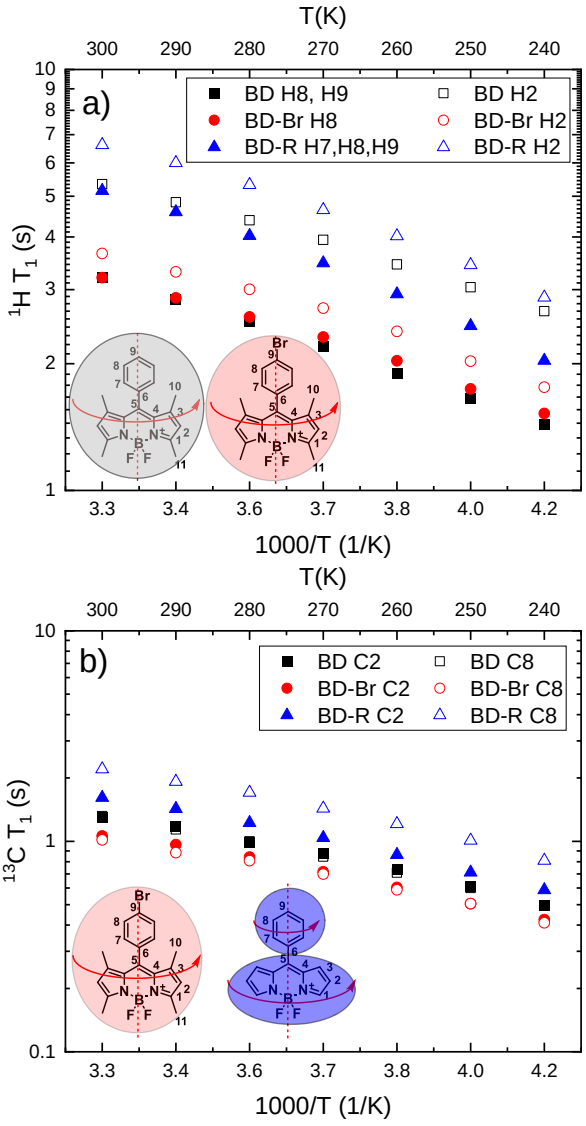

Figure. 5. Comparison of selected T_1 values as a function of temperature a)$^{1}HT_1$ and b) $^{13}CT_1$. Inset: Proposed rotational motion of BD, BDBr and BDR.

In Figure. 5a, $^{1}HT_1$ of phenyl protons (H7, H8 and H9) in BDR are twice as long as the ones in BD which has almost the same $^{1}HT_1$ as BDBr. This behavior indicates that the phenyl groups in BDR rotate faster

than the ones in BD or BDBr because of the absence of methyl groups that hinder the phenyl rotation. Moreover, $^{1}HT_1$ of H2 in all of the molecules is longer than the ones in the phenyl moiety suggesting that H2 rotates rapidly and it is the farthest from the rotation axis. Thus, $^{1}HT_1$ measurements indicate that BD and BDBr have the same rotational speed but rotation in BDR is even faster. Thus, if a small molecule tumbles rapidly, the DD relaxation is less effective and T_1 becomes longer.

The $^{13}CT_1$ measurements of BD, BDBr and BDR in Figure. 5b corroborates the behavior observed by $^{1}HT_1$ measurements. $^{13}CT_1$ of C2 of the BDBr exhibits the shortest value while the ones in BDR have the longest. Therefore, the rotational speed of the molecules is as follows BDR > BD > BDBr. Moreover, $^{13}CT_1$ values of the phenyl carbons (C7, C8 and C9) indicate that the rotational speed of these carbons is similar to that in C2, except for BDR, which is higher. Thus, BDBr has an isotropic motion similar to BD while BDR presents an anisotropic motion where the phenyl moiety rotates faster that the BODIPY fragment.

Assuming that the dipole-dipole relaxation mechanism is the only one that contributes to the ^{13}C relaxation times of protonated carbons, Table 1 shows the $^{13}CT_1$ derived parameters from the BPP theory, eq. 1-6. Regardless of the absence of a minimum in the $^{13}CT_1$ *vs* temperature curves, all protonated carbons T_1 fit well the Arrhenius-type BPP behavior.

Table 1. Derived parameter from BPP theory for meso-phenyl BODIPYs.

atom	BD		BDBr		BDR	
	E_a (kJ/mol)	τ_0	E_a (kJ/mol)	τ_0	E_a (kJ/mol)	τ_0
1					10.4	1.72E-13
2	9.5	2.60E-13	9.8	1.46E-13	10.2	1.59E-13
3					10.2	1.76E-13
7	9.8	2.29E-13	9.3	1.75E-13	9.7	1.39E-13
8	9.4	2.89E-13	8.8	2.26E-13	9.8	1.37E-13
9	9.3	3.37E-13			9.8	2.27E-13
10			8.4	5.91E-14		
11			8.4	5.87E-14		

The temperature dependences of τ_c of all the carbons in the phenyl moiety and C2 carbons are close. For example, at 300 K, $\tau_c = 1x10^{-11}$ s for BD and $\tau_c = 8x10^{-12}$ s for BDBr. However, in BDR $\tau_c = 7x10^{-12}$ s for phenyl carbons and $\tau_c = 9x10^{-12}$ s for C2. These values are typical for small molecules in non-viscous solutions.[17]

The activation energies (E_a) of the molecular reorientation of phenyl carbons are around 9.5 kJ/mol for BD, 9.0 kJ/mol for BDBr and 9.8 kJ/mol for BDR. The E_a values for C2 are 9.5, 9.8 and 10.2 kJ/mol, respectively. These E_a values are similar to $^{13}CT_1$ studies in ionic liquids where fluctuations of functional groups and methyl rotations were present.[18] Moreover, E_a values in T_1 relaxation studies are associated to molecular confinement measurements, intermolecular interactions and environmental effects around the molecule.[19] The mean values of E_a in BD, BDBr and BDR are 9.5 kJ/mol, 8.9 kJ/mol and 10.0 kJ/mol, respectively.

Conclusion

Calculations with quantum chemistry by using GIAO-DFT level of theory allowed to assign protons and carbons with high confidence in experimental ^{1}H and ^{13}C spectra. The $^{1}HT_1$ and $^{13}CT_1$ relaxation measurements of *meso*-phenyl BODIPYs diminish with the temperature reduction without reaching a minimum in the range of 240-300 K. $^{1}HT_1$ and $^{13}CT_1$ measurement aided to propose a rotational model where the rotational axis is located between atom C9 and boron. Moreover, *BD and BDBr rotate as a sphere with an isotropic rotational motion*. However, BDR shows an anisotropic motion where the phenyl moiety has high rotation compared to BD and BDBr. BPP theory was used considering dipole-dipole as the main T_1 relaxation mechanism and the derived parameters (τ_c and E_a) confirmed the isotropic and anisotropic motions found experimentally. The mean values of E_a in BDR, BD and BDBr are 9.5 kJ/mol, 8.9 kJ/mol and 10.0 kJ/mol, respectively.

References

[1] U. Ziener, A. Godt, Synthesis and Characterization of Monodisperse Oligo(phenyleneethynylene)s, *J. Org. Chem.* **62** (1997) 6137–6143, https://doi.org/10.1021/jo970548x

[2] A. Loudet, K. Burgess, BODIPY dyes and their derivatives: Syntheses and spectroscopic properties, *Chem. Rev.* **107**, (2007) 4891–4932, https://doi.org/10.1021/cr078381n

[3] Y. Hou, I. Kurganskii, A. Elmali , H. Zhang, Y. Gao, L. Lv, J. Zhao, A. Karatay, L. Luo, M. Fedin, Electronic coupling and spin–orbit charge transfer intersystem crossing (SOCTISC) in compact BDP–carbazole dyads with different mutual orientations of the electron donor and acceptor, *J. Chem. Phys.* **152** (2020) art. 114701, https://doi.org/10.1063/1.5145052

[4] S. Zappia, A. de León, M. Alloisio, E. Arias, G. Dellepiane, G. Petrillo, I. Moggio, S. Thea, C. Gallardo, M. Rodríguez, Optoelectronic Properties of a Perylene substituted (Cholesteryl)benzoateethynylene co-polymer, *Mat. Chem. Phys.* **147** (2014) 476-482, https:/doi.org/ 10.1016/j.matchemphys.2014.05.017

[5] H.-Y. Lin, W.-C. Huang, Y.-C. Chen, H.-H. Chou, C.-Y. Hsu, J.T. Lin, H.-W. Lin, BODIPY dyes with β-conjugation and their applications for high-efficiency inverted small molecule solar cells, *Chem. Commun*. **48** (2012) 8913–8915, https://doi.org/10.1039/C2CC34286C

[6] S. A. El-Daly, S. A. El-Azim, F. M. Elmekawey, B. Y. Elbaradei, S. A. Shama, A. M. Asiri, Photophysical Parameters, Excitation Energy Transfer, and Photoreactivity of 1,4-Bis(5-phenyl-2-oxazolyl)benzene (POPOP) Laser Dye, *Int. J. Photoenergy* (2012), art. 458126, https://doi.org/10.1155/2012/458126

[7] X. Liu, W. Chi, Q. Qiao, S.V. Kokate, E. Peña Cabrera, Z. Xu, X. Liu, X. Liu, Y.-T. Chang, Molecular Mechanism of Viscosity Sensitivity in BODIPY Rotors and Application to Motion-Based Fluorescent Sensors, *ACS Sens.* **5** (2020) 731–739, https://doi.org/10.1021/acssensors.9b01951

[8] W. Miao, C. Yu, E. Hao, L. Jiao, Functionalized BODIPYs as Fluorescent Molecular Rotors for Viscosity Detection. *Front. Chem.* **7** (2019) 1–6, https://doi.org/10.3389/fchem.2019.00825

[9] C. Wiedemann, G. Hempel, F. Bordusa, Reorientation dynamics and ion diffusivity of neat dimethylimidazolium dimethylphosphate probed by NMR spectroscopy, *RSC Adv.* **9** (2019) 35735–35750 (2019), https://doi.org/ 10.1039/c9ra07731f

[10] A. Gradišek, M. Cifelli, M. Wojcik, T. Apih, S.V. Dvinskikh, E. Gorecka, V. Domenici, Study of liquid crystals showing two isotropic phases by 1 H NMR diffusometry and 1 H NMR relaxometry, *Crystals* **9** (2019) art. 178, https://doi.org/10.3390/cryst9030178

[11] R. S. Norton, R. P. Gregson, R. J. Quinn, N.M.R. spin-lattice relaxation time measurements determining the major tautomer of 1-methylisoguanosine in solution, *J. Chem. Soc. Chem. Commun.* **8** (1980) 339–341, https://doi.org/10.1039/C39800000339

[12] B. Rodríguez-Molina, S. Pérez-Estrada, M. A. Garcia-Garibay, Amphidynamic crystals of a steroidal bicyclo[2.2.2]octane rotor: A high symmetry group that rotates faster than smaller methyl and methoxy groups, *J. Am. Chem. Soc.* **135** (2013) 10388–10395, https://doi.org/10.1021/ja4024463

[13] A. M. Huynh, A. Müller, S. M. Kessler, S. Henrikus, C. Hoffmann, A. K. Kiemer, A. Bücker, G. Jung*et,* Small BODIPY Probes for Combined Dual19F MRI and Fluorescence Imaging,

ChemMedChem **11** (2016) 1568–1575, https://doi.org/10.1002/cmdc.201600120
[14] F. Neese, Software update: The ORCA program system—Version 5.0, *WIREs Computational Molecular Science* **12** (2022) art. e1606, https://doi.org/10.1002/wcms.1606
[15] M. E. di Pietro, F. Castiglione, A. Mele, Polar/apolar domains' dynamics in alkylimidazolium ionic liquids unveiled by the dual receiver NMR 1H and 19F relaxation experiment. *J Mol Liq* **322** (2021) art. 114567, https://doi.org/10.1016/j.molliq.2020.114567
[16] R. G. Parker, J. Jonas, Spin-Lattice Relaxation in Several Molecules Containing Methyl Groups, *J. Magn. Reson (1969)* **6** (1972) 106-116, https://doi.org/10.1016/0022-2364(72)90091-1
[17] R. Witt, L. Sturz, A. Dölle, F. Müller-Plathe, Molecular dynamics of benzene in neat liquid and a solution containing polystyrene.13C nuclear magnetic relaxation and molecular dynamics simulation results, *J. Phys. Chem. A* **104** (2000) 5716–5725, https://doi.org/10.1021/jp000201p
[18] Y. Shimizu, Y. Wachi, K. Fujii, M. Imanari, K. Nishikawa, NMR Study on Ion Dynamics and Phase Behavior of a Piperidinium-Based Room-Temperature Ionic Liquid: 1-Butyl-1-methylpiperidinium Bis(fluorosulfonyl)amide, *J. Phys. Chem. B* **120** (2016) 5710–5719, https://doi.org/10.1021/acs.jpcb.5b07346
[19] R.J. Foster, R. A. Damion, M. E. Ries, S. W. Smye, D. G. McGonagle, D. A. Binks, A. Radjenovic, Imaging of nuclear magnetic resonance spin-lattice relaxation activation energy in cartilage. *R. Soc. Open Sci.* **5**, (2018) art. 180221, https://royalsocietypublishing.org/doi/10.1098/rsos.180221